ACS SYMPOSIUM SERIES 732

Modeling NMR Chemical Shifts

Gaining Insights into Structure and Environment

Julio C. Facelli, EDITOR
University of Utah

Angel C. de Dios, EDITOR
Georgetown University

American Chemical Society, Washington, DC

Chapter 23

Application of Nuclear Shielding Surfaces to the Fundamental Understanding of Adsorption and Diffusion in Microporous Solids

Cynthia J. Jameson[1], A. Keith Jameson[2], Angel C. de Dios[3], Rex E. Gerald II[4], Hyung-Mi Lim[5], and Pavel Kostikin[1]

[1]Department of Chemistry, University of Illinois at Chicago, Chicago, IL 60607
[2]Department of Chemistry, Loyola University, Chicago, IL 60626
[3]Department of Chemistry, Georgetown University, 37th and O Streets, NW, Washington, DC 20057
[4]Argonne National Laboratory, Argonne, IL 60439
[5]Chonnam National University, Chonnam, South Korea

The intermolecular chemical shift provides a means by which very detailed questions can be answered towards a fundamental understanding of two basic processes in the many technological applications of microporous materials: adsorption and diffusion. We demonstrate that the detailed equilibrium properties of physisorbed small molecules and the rates of cage-to-cage migration in zeolites can be observed and quantitatively reproduced by theoretical calculations. Some of the questions which have been answered include: When molecules are adsorbed in a microporous solid at a given loading, what fraction of the cavities have exactly n molecules? How many molecules of type 2 can be found in those cavities that have exactly n molecules of type 1? How do the type, size, and locations of cations affect the distribution of molecules within a microporous solid? How is the NMR chemical shift affected by confinement with n molecules of another type in a cavity? A zeolite cage provides a model system for the understanding of solvent effects on chemical shifts, for the theoretical investigation of the temperature dependence of medium chemical shifts under constant volume conditions in which very detailed comparisons with experiment can be carried out.

Microporous solids, zeolites in particular, are widely used in heterogeneous catalytic processes, separations, oil recovery, and other industrial processes (*1*). A microscopic

understanding of elementary processes at surfaces, such as adsorption and diffusion is an important fundamental problem and may assist in interpreting more complicated surface chemistry. A simple rare-gas physisorption system is a good starting point to investigate the distribution and dynamic behavior of adsorbed species. We use a combination of NMR spectroscopy and computer simulations in fundamental studies of adsorption and diffusion. ^{129}Xe NMR is widely used in the characterization of microporous materials. In zeolites (*2-5*), polymers (*6-8*), coals (*9*), clays (*10*) and other porous materials (*11*), the mobility of the Xe atoms is such that only one Xe signal is usually observed in the NMR spectrum. The average chemical shift of the single peak under fast exchange and its dependence on the temperature and the average Xe occupancy are all that can be observed in nearly all microporous solids. In these cases the Xe chemical shift is known empirically to depend on zeolite pore and channel dimensions (*12-15*), location of cations (*16*), co-adsorbed molecules (*17,18*), dispersed metal atoms (*1,4,5*) and paramagnetic ions (*19,20*), on water content (*21*), blockage of pores by coking (*22*), domains of different composition or crystallinity (*23*), etc.

The Model System

We choose to carry out systematic studies in specifically those zeolites (type *A*) of known structure where the position of every Si and Al atom and also every charge-balancing cation is known, where the actual equilibrium distribution of cages containing specifically known numbers of Xe atoms is directly observed, where the average chemical shift of ^{129}Xe in cages containing a specific number of Xe atoms is individually observable, as well as its temperature dependence, and where the temperature dependence of the average Xe occupancy (the adsorption isotherm) can also be observed at the same time. For our model system we have chosen zeolite Na*A*. This is an aluminosilicate of formula $Na_{12}[(SiO_2)_{12}(AlO_2)_{12}]$ whose crystal structure is well characterized. The framework structure provides a simple cubic arrangement of contiguous large cages (alpha cages). A Na^+ ion in each of the 6 windows to the cages keep the Xe atoms adsorbed inside for sufficiently long residence times such that each Xe_n is observed as a distinct signal in the high resolution NMR spectrum. By making measurements in such a system, for example, pure Xe in Na*A*, or a mixture of Xe and other sorbate molecules in competitive adsorption in zeolite Na*A*, we expect to be able to obtain directly from experiment, information about adsorption and diffusion not otherwise available. These observations provide direct tests of those details of computer simulations that are usually averaged over. These provide more critical and detailed constraints on the computer modeling than otherwise.

Observations

The most interesting and challenging experimental data to be interpreted are the chemical shifts observed in the Xe, Xe_2, Xe_3, ..., Xe_8 clusters trapped in the alpha cages of the zeolite Na*A* (*24,25*). Here, what is observed is not an average chemical shift under fast exchange of the Xe with a very large number of cavities containing a variable number of Xe atoms, but rather the individual chemical shifts of trapped clusters of Xe atoms, Xe_1, Xe_2, Xe_3,... up to Xe_8. The chemical shifts have been

measured as a function of temperature (*24*) and these pose a dynamical averaging challenge for the theory. The shielding of the ^{129}Xe in the Xe_n clusters changes according to n; the most deshielded nuclei are in the Xe_8 cluster, but the individual cluster shifts do not change with loading. The cluster shift is in the direction given by $\sigma_1(T)$ observed in the gas phase, however, the incremental change is not a fixed amount but increases slightly in going from 1 to 6. Furthermore, there is a big change in shielding in going from Xe_6 to Xe_7 and then again in going from Xe_7 to Xe_8. These individual Xe_n peaks are also observed experimentally in zeolite K*A* (*26*)and in zeolite Ag*A* (*27*). The net effect of the larger cation size on the Xe_n clusters (found experimentally) is to increase the chemical shift and enhance the increments [$\delta(Xe_n)$ - $\delta(Xe_{n-1})$] (compared to zeolite Na*A*). Under magic angle spinning, it has been possible to narrow the peaks corresponding to the Xe_n clusters in zeolite cages oriented in various directions relative to the magnetic field (*28*) . With very narrow lines it has been possible to distinguish by their different intermolecular shifts the Xe_n signals in the distinguishable cages that arise upon substitution of Ca^{2+} ions for Na^+ ions in the same zeolite: The progression of Xe_n signals associated with each cage type can be observed. (Incidentally, they have somewhat different distributions, as can be observed from the Xe_n intensities.)(*28*) This is a dramatic illustration of the sensitivity of the ^{129}Xe shielding to the environment.

In studies of competitive adsorption, the usually measured quantity is the overall composition of the adsorbed phase for a given composition of the bulk phase in equilibrium with it. It has been found that chemical shifts can provide a more detailed description. In a mixture of Xe and Kr in Na*A* zeolite it was possible to observe the individual signals from Xe_nKr mixed clusters as well as the Xe_n clusters under magic angle spinning (*28*). The absolute ^{129}Xe chemical shifts of the Xe_nKr mixed clusters and the increments between Xe_nKr and the Xe_{n+1} in various Xe-Kr mixtures in Na*A* zeolite, are shown in Table I.

Table I. ^{129}Xe chemical shifts of mixed clusters Xe_nKr in the alpha cages of zeolite Na*A* (ppm)

	$\delta(Xe_nKr)$		$\delta(Xe_nKr) - \delta(Xe_n)$	
Cluster	*OBSD*[a,b]	*GCMC*[a,b]	*OBSD*	*GCMC*[b]
Xe_1Kr	84.7	85.7	9.9	8.6
Xe_2Kr	103.3	102.6	11.0	9.9
Xe_3Kr	124.5	121.3	12.8	11.6
Xe_4Kr	148.9	144.3	15.7	14.4
Xe_5Kr	174.7	172.0	16.3	16.8
Xe_6Kr	209.9	209.1	26.5	25.1

[a] relative to an isolated Xe atom, Ref. (*28*). [b] Ref. (*29*).

In the competitive adsorption of Xe and Ar in Na*A* zeolite, the Ar atoms are in fast exchange, so that individual mixed clusters like Xe_nAr_m can not be observed. Here, the Xe_n peaks are observed just as in pure Xe in this zeolite, except that the individual chemical shifts are observed to be dependent on the loadings of Ar (primarily) and Xe (secondarily) (*30*). Here the total intermolecular chemical shift

measured relative to the isolated Xe atom, the ^{129}Xe chemical shift for Xe_n in an alpha cage with an average number of Ar atoms under fast exchange. The differences in shielding, $[\langle\sigma(Xe_nAr_{ave})\rangle - \langle\sigma(Xe_n)\rangle]$, obtained directly from experiment, are a direct measure of the intermolecular effects of Ar, and are therefore a direct measure of the average number of Ar atoms in the cage with Xe_n. Similarly, for mixtures of Xe with CH_4, N_2, CO_2 or CO, the differences in the shielding of the Xe_n peak in the mixture sample and the corresponding Xe_n peak in the pure Xe sample is a direct measure of the average number of molecules of, respectively, CH_4, N_2, CO_2, or CO, in the same cage as the *n* Xe atoms. To extract this average number for every Xe_n in any such coadsorbed mixture in zeolite Na*A*, at any mole fraction of the constituent gases in the bulk gas in equilibrium with the molecules adsorbed inside the zeolite, we require the Xe-CH_4, XeN_2, Xe-CO_2, and Xe-CO intermolecular shielding surface.

Intermolecular Shielding Surfaces

An intermolecular shielding surface is a mathematical function describing the dependence of the nuclear shielding as a function of the configuration of two interacting molecules. Some shielding surfaces have been calculated for interacting rare gas pairs (*31*), and rare gas atoms interacting with cations, diatomic molecules, or H_2O (*32*), and for dimers and n-mers of H_2O molecules (*33,34*).

Shielding Surfaces for Two Interacting Molecules. In the Maryland meeting Jameson and de Dios reported the first ab initio calculations of the rare gas pair intermolecular shielding surfaces for Ar_2, ArNe, Ne_2, and NeHe (*35*). With these shielding surfaces it was possible to calculate the second virial coefficient for nuclear shielding as a function of temperature, using the well established intermolecular potential functions $V(R)$ for the pair.

$$\sigma_1(T) = \int_0^\infty 4\pi R^2 dR\, [\sigma(R) - \sigma(\infty)] \exp[-V(R)/k_BT].$$

It had been found that the shielding functions are nearly conformal in the range $\infty > R > r_0$.and that the scaling factors relating intermolecular shielding functions of rare gas pairs are $\langle a_0^3/r^3\rangle_1\ \alpha_1(0)\ U_1U_2/(U_1+U_2)$, with the R scaling according to r_0. The values of $\langle a_0^3/r^3\rangle_{np}$ for the free atom, the static electric dipole polarizability $\alpha(0)$ and the ionization potentials, U are well known for the rare gas atoms, which permit the scaling of the Ar-Ar shielding function to any of the rare gas pairs. The calculation of $\sigma_1(T)$ for Xe-Xe, Xe-Kr, and Xe-Ar could therefore be carried out and the results could be compared with the experimentally measured density coefficients of nuclear shielding $\sigma_1(T)$ for these pairs. The ab initio calculations of the shielding function at the RPA level was found to be very close to that obtained at the level of SOPPA, using LORG and SOLO methods (localized orbitals/local origins and second order localized orbitals/local origins) respectively (*31*). These earlier calculations are validated by more recent results. It has been found, more recently, that the Ne-Ne intermolecular shielding function calculated at the SCF-GIAO level is nearly indistinguishable from that calculated at the CCSD(T) level for the range 2.2 - 4.0 Å where r_0 = 3.07 Å (Bühl, M.; Kaupp, M.; Malkin, V. G.; Malkina, O. L. *J. Comp. Chem.*, **1999**, in press.). It appears that the difference between the Hartree-Fock and the highest level of electron correlation for the intermolecular shielding function of

the rare gas pair is indeed small. Also, it has been found (de Dios and Jameson, to be published) that the ab initio Xe-Xe intermolecular shielding function is very close to the Xe-Xe function obtained by scaling the ab initio Ar-Ar shielding function in the range $4r_0$ Å > R > $0.9r_0$. The new Xe-Xe shielding function was calculated using a large Xe atom basis set (240 basis functions), large enough that the counterpoise correction to the intermolecular shielding is negligibly small.

For Xe interacting with molecules N_2, CO and CO_2, the ^{129}Xe shielding functions have been calculated (*36*) as a function of two variables, the center of mass distance and the angle θ that the linear molecule axis makes with the center-of-mass-distance vector. Here, too, the counterpoise correction to the shielding function is very small, indicating that the Xe basis set used is large enough. These intermolecular shielding functions have been used to calculate the second virial coefficients of ^{129}Xe shielding for the pairs Xe-N_2, Xe-CO, and Xe-CO_2. When using presently available interaction potential functions, V(R,θ), the comparisons of calculated and experimental $\sigma_1(T)$ values reveal good agreement with the temperature behavior of all three pairs, and good agreement with trends in relative magnitudes of these three compared with each other and with Xe-Xe, Xe-Kr and Xe-Ar values, although the recovery of absolute magnitudes is not complete. Improved potentials are clearly necessary.

To describe the numerical results of the ab initio shielding calculations, a choice of functional form is required to represent the shielding surface in analytic form. For the rare gas pair, it was found that the inverse R dependence of σ (R) has a behavior close to $R^{-6.7}$, $R^{-6.8}$, and $R^{-7.4}$. Therefore, a function of the form

$$\sigma(R) - \sigma(\infty) = \sum_n a_n R^{-n}$$

with n = even only, 6 up to 12 or 14, would appear to be an adequate description. The coefficients a_n are obtained by least squares fitting to the ab initio values at various R. On the other hand, for the Xe-linear molecule interaction, a_n may be taken to be a function of the angle θ, reflecting the symmetry of the system, such as

$$a_n = \sum_{\lambda=0,even} a_{n\lambda} P_\lambda(\cos\theta)$$

with λ = 0, even only, up to 6 or 8 for Xe-N_2 and Xe-CO_2, or λ = 0, 1, 2, 3, 4... for Xe-CO. The coefficients $a_{n\lambda}$ are found by least squares fitting to the ab initio values of σ(R,θ) that have been calculated at intervals of 15°. An alternative description is

$$\sigma(R) - \sigma(\infty) = \sigma(R_{Xe\text{-}O}) + \sigma(R_{Xe\text{-}O'}) + \sigma(R_{Xe\text{-}C})$$

$$\sigma(R_{Xe\text{-}O}) = \sum_n a_n^{(Xe\text{-}O)} R_{Xe\text{-}O}^{-n}$$

$$\sigma(R_{Xe\text{-}C}) = \sum_n a_n^{(Xe\text{-}C)} R_{Xe\text{-}C}^{-n}$$

where a pairwise additive form is used. For more complex interacting molecules, where it is not feasible to find a simple description in terms of Legendre expansions, the pairwise additive form is the functional form of choice.

Shielding Surfaces for a Molecule Adsorbed on a Zeolite Fragment. Since the Xe is adsorbed onto an inner surface of the zeolite, it would be ideal to include the entire zeolite cage framework atoms and ions in the calculations. However, this size calculation is not yet feasible, thus, only a fragment of the cage is used. For this purpose, a fragment terminated with $OSi(OH)_3$ groups rather than the more commonly used $OSiH_3$ groups is used. All atoms are placed at the atomic coordinates

obtained from high resolution x-ray or neutron scattering. Counterpoise corrections are required for each ab initio calculation of the supermolecule with various positions of the adsorbed Xe atom. This is crucial here, because the zeolite framework atoms and ions provide a large number of additional orbitals in which the electrons of the rare gas atom may be found, effectively increasing the basis set size in going from isolated rare gas atom to the supermolecule. A pairwise additive functional form is practical here, in terms of the distance between the rare gas atom and each O atom and each Na^+ ion. These calculations have been reported by Jameson and Lim for a zeolite with a 1:1 ratio of Si to Al in the framework and various charge-balancing cations.(*37*).

Computational Methods

The grand canonical ensemble is appropriate for adsorption systems, in which the adsorbed phase is in equilibrium with the gas at some specified temperature. The use of a computer simulation allows us to calculate average macroscopic properties directly without having to explicitly calculate the partition function. The grand canonical Monte Carlo (GCMC) method as applied in this work has been described in detail earlier (*38*) . The aspects involving binary fluid mixtures have been described previously in our Xe-Ar work (*30*).

Cut-and-shifted effective potentials describe the interaction between the adsorbed fluid and the zeolite. The Xe-O and Xe-Na parameters are unchanged from our previous work on Xe in Na*A* (*38*) and Xe-Ar mixtures in Na*A* (*30*). The Kr-O and Kr-Na potential parameters were obtained as described in Ref. (*29*). The CH_4-O and CH_4-Na potential surfaces were described by the pairwise Lennard-Jones parameters given by Woods and Rowlinson (*39*).

The Xe-Xe potential used is of the Maitland-Smith form, as described in our previous simulations of Xe in Na*A* (*38*), fitted to the best available Xe-Xe potential of Aziz and Slaman (*40*). Likewise the Xe-Kr and the Kr-Kr potentials were taken from the best available potentials of Aziz *et al.* (*41, 42*), and fitted to the Maitland-Smith form. The Xe-CH_4 and the CH_4-CH_4 potential functions used were of the atomic site-site form based on the best available potentials of Liuti et al and Righini et al. respectively (*43, 44*).

The simulation box is a unit cell of zeolite Na*A*, with the atomic coordinates, including the Na cations, taken from the x-ray single crystal refinement of the dehydrated zeolite by Pluth and Smith (*45*). Periodic boundary conditions were imposed using the minimum image convention, consistent with the cut-and-shifted potentials employed (*46*). The core of the program effects the creation/destruction and displacement of one molecule at a time and calculates the associated energy change, ΔU in each case. This is used to continuously update the total configurational energy of the system, without having to recalculate every interaction at every step. The displacement step uses the adsorbed phase composition in the choice of either fluid. The creation/destruction step begins with the decision to either create or destroy a particle. If the decision is to destroy a particle (that is, the particle is assumed to go into the gas phase) the choice between destroying a molecule of Xe or CH_4 is made proportionately to the gas phase composition, i.e., ρ_{Xe} and ρ_{CH4} . ;likewise, the choice of creating a molecule of Xe or CH_4 (i.e., remove it from the bulk gas and place it in the zeolite) is made according to the gas phase composition. It is necessary to know *a priori* the ratio of the gas densities in equilibrium with the adsorbed phase before the simulation starts. This is easily done by first calculating the chemical potential of the Xe and the CH_4 appropriate to the temperature and densities in the gas mixture, using the virial coefficients (*30*). These chemical potentials, the temperature, and the mole fraction of Xe in the gas are the parameters of a GCMC simulation.

In our approach, the ^{129}Xe shielding, like the energy, is taken to be expressible as a sum of pairwise contributions, using atom-atom shielding functions that are likewise cut and shifted. The Xe-O and Xe-Na shielding functions are based on *ab initio* calculations on model systems and are the same as was used in our previous work (*30,38*). The Xe-Xe and the Xe-Kr shielding functions are based on *ab initio* calculations and are taken from Ref. (*32*). The Xe-CH_4 shielding functions are based on ab initio calculations at three symmetrical orientations of the CH_4 molecule relative to the rare gas taken at various distances and fitted to shielding contributions from H and C centers (*47*). These have been shown to reproduce reasonably well the temperature dependent density coefficients of the ^{129}Xe chemical shifts for pure xenon gas and for Xe in Kr, and Xe in CH_4 gas mixtures. At each step in the simulation at which the atom-atom interaction energy is calculated, the shielding contribution is calculated too, when one of the atoms involved is a xenon atom. Since the shielding functions go to large negative values at close approach, it is quite important to have Xe-Xe, Xe-Kr and Xe-CH_4 potentials that have the correct behavior at these short distances, especially close to r_0. This is the reason for using as accurate two-body potentials as possible for Xe-Xe and Xe-Kr or Xe-CH_4. The Maitland-Smith form provides a superior fit to the best rare gas pair potentials and is just as inexpensive as the Lennard-Jones form in computational overhead. The Maitland Smith form is also used for the Xe-C and Xe-H parts of the Xe-CH_4 potential.

The results of the GCMC simulations are analyzed to provide the usual averages for each (μ_{CH4}, μ_{Xe},T), such as $\langle n \rangle_{Xe}$, $\langle m \rangle_{Kr}$, the average number of atoms per alpha cage, the xenon distribution, P_n, i.e., the fractions of the cages that are occupied by n Xe atoms, as well as the detailed occupancies $f(Xe_nKr_m)$, i.e., the fractions of the cages that are occupied by n Xe atoms and m Kr atoms. In addition, the one-body distribution functions, pair distribution functions, and average shieldings for individual mixed clusters Xe_nKr_m or $Xe_n(CH_4)_m$, which are independent of loading, are accumulated over all the GCMC runs. All calculations reported here were carried out on IBM RISC/6000 (models 560 and 365) workstations.

Given that the total potential energy is a sum over all the pairwise interactions at distances less than some cutoff distance, and given the interaction potential function for the Xe-other sorbate interactions, likewise taken to be pairwise additive, then the properly weighted large number of configurations (a million or so) can be summed in a Grand Canonical Monte Carlo (GCMC) scheme (*38*). At each of these configurations the shielding of every Xe nucleus is calculated. Ab initio shielding calculations for ^{39}Ar in the triangular and linear Ar_3 clusters have shown that as long as the Ar atoms do not get much closer than about $0.9r_0$, the isotropic shielding contributions can be obtained by additivity. We therefore construct the ^{129}Xe shielding surface as we go, summing up over all the atoms that are sufficiently close (less than 12 Å). The approach is to treat the whole system (any number of Xe atoms per unit cell and atoms of the zeolite framework) as a supermolecule and to calculate

the shielding function at each configuration by assuming that the intermolecular shielding is pairwise additive, that is, for a given ^{129}Xe nucleus the shielding is a sum of contributions from Xe-Xe as a function of distance to all the other Xe atoms, plus Xe-O as a function of distance to all the O atoms of the zeolite framework, plus Xe-Na^+ as a function of distance to all the Na^+ counterions. The Xe-Al and Xe-Si contributions are neglected; the Xe atom can not get close to these atoms due to the O atoms bridging the Al and Si. The shielding surface is thus constructed on the fly, using the pair shielding functions $\sigma(Xe\text{-}O_{zeo})$, $\sigma(Xe\text{-}Na_{zeo})$ and $\sigma(Xe\text{-}Xe)$ derived from ab initio calculations described above (*31, 37*), changing with the numbers of neighbors as the numbers of sorbate atoms fluctuate in the grand canonical ensemble. The isotropic ^{129}Xe shielding averaged over all the Xe atoms in a cluster are separately stored for each of the eight cluster types so that the average chemical shift for each Xe_n can be obtained. This is done at each temperature. The averages at various temperatures can then be compared with the experimental chemical shifts at these temperatures (*38*).

Results

The distributions of the Xe atoms among the cages of the zeolite are provided by the relative intensities of the Xe_1, Xe_2, Xe_3, ...Xe_8 peaks seen individually in the ^{129}Xe NMR spectrum. Thus, the NMR experiment provides a direct measure of the distribution of Xe atoms among the cavities, e.g., what fraction of the zeolite cages have 5 exactly Xe atoms? This is reproduced very well by the grand canonical simulations described above.

The calculated and experimental quantities being compared are in absolute terms, that is, the shieldings are relative to the free Xe atom in both calculation and experiment. The agreement of the GCMC average with experiment is excellent, especially considering that there are no adjustable parameters once the Xe-zeolite potential parameters are adopted. That the increments between the Xe_n cluster shifts are well-reproduced, including their temperature dependence, might have been expected from the good agreement found in the gas phase chemical shifts based on the same ab initio-derived Xe-Xe intermolecular chemical shift function, since these chemical shift increments are largely due to the Xe-Xe interactions.

What about the changes in the intermolecular chemical shifts when the atoms of the zeolite cage are changed? The GCMC simulations permit examination of the separate contributions coming from the cations, the zeolite framework (effectively represented by the O atoms), and Xe-Xe contributions. The difference between the Xe-O and Xe-cation contributions in K*A* and Na*A* is interesting since the same $\sigma(Xe...O_{zeol})$ and $V(Xe\text{-}O_{zeol})$ functions were used in the GCMC simulations in both zeolites. The direct cation contribution to the chemical shift is larger for K than for Na in all cluster sizes, and this increases with cluster size. This is more pronounced in the K*A* cage due to the in-out arrangements of the K ions (*26*). The excluded volume effect due to the latter leads to smaller Xe-O contributions in K*A* and larger contributions from the Xe-Xe interactions, becoming more severe with increasing number of Xe atoms due to the more pronounced deshielding exhibited by the $\sigma(r_{Xe\text{-}Xe})$ function at shorter distances. Although the calculated numbers can and do change upon changing the parameters of the V(Xe-K) potential, the trends are all preserved.

The calculated differences between the chemical shift of Xe_n in K*A* and Na*A* are in semi-quantitative agreement with experiment, and the GCMC simulations reproduce the trends for the temperature dependence of the ^{129}Xe chemical shifts of the Xe_n clusters in K*A* (*26*) just as well as they did for Xe_n in Na*A* (*38*). The GCMC averaging for Xe_n in partially Ca^{2+} ion-exchanged Na*A* also reproduce the chemical shift increments assigned to cages having 1 or 2 Ca^{2+} ions. Polarization terms in the energy of Xe due to interactions with cations, a non-pairwise additive potential energy term, had to be included to take into account the differences in mono- versus di-valent cations (*48*).

The absolute ^{129}Xe chemical shifts of the Xe_nKr mixed clusters and the increments between Xe_nKr and the Xe_{n+1} are reproduced by GCMC averaging in various Xe-Kr mixtures in Na*A* zeolite, as shown in Table I. In Figure 1 we compare the experimental Xe_n cluster chemical shifts in 9 different samples of Xe-CH_4 mixtures in Na*A* with the average chemical shifts from the GCMC simulations with the same overall $\langle n \rangle_{Xe}$ and $\langle m \rangle_{CH4}$ as experiment. Here the total intermolecular chemical shift measured relative to the isolated Xe atom, the ^{129}Xe chemical shift for Xe_n in an alpha cage with an average number of CH_4 molecules under fast exchange (which is directly calculated in the GCMC simulation) is plotted in comparison with the experimental values. We see that in an absolute measure, the calculated chemical shifts are in very good agreement with experiment. Furthermore, the differences in shielding, $[\langle \sigma(Xe_nCH_{4\ \langle m \rangle}) \rangle - \langle \sigma(Xe_n) \rangle]$, may be compared directly with experiment, are a direct measure of the intermolecular effects of CH_4, and are therefore a direct measure of the average number of CH_4 molecules in the cage with *n* Xe atoms. These calculated shielding differences are in quantitative agreement with experiment for samples with various Xe and CH_4 loading (*47*). The simulations also provide the average number of CH_4 molecules associated with each individual Xe_n. Once the average ^{129}Xe chemical shifts in the $Xe_n(CH_4)_m$ mixed cluster chemical shifts have been calculated for each *n* and *m* combination in the GCMC simulations, the Xe_n chemical shifts observed in any sample of Xe-CH_4 mixtures in zeolite Na*A* can be converted directly to the average number of CH_4 molecules in the same cage with *n* Xe atoms while the fraction of cages containing exactly *n* Xe atoms is directly given by the relative intensity of the Xe_n peak. In other words, the ^{129}Xe chemical shifts provide the detailed distribution of the Xe-CH_4 mixture among the cavities of the zeolite. Other mixtures (Xe-CO, Xe-CO_2, Xe-N_2,...) can be studied in this way.

The ^{129}Xe chemical shifts of each of the peaks associated with Xe_1, Xe_1Kr_1, Xe_2, Xe_2Kr_1, ...Xe_6Kr_1, ...Xe_8 are observed individually. On the other hand, because Ar or CH_4 are freely migrating from one cage to the next, only an average occupancy of Ar or CH_4 is seen by the Xe nuclei. Thus, only an average Xe_n NMR chemical shift is observed, differing from that of the Xe_n peak when pure xenon is trapped in the zeolite, by an amount which is directly related to the average number of Ar or CH_4 molecules (visiting sorbates) in the same cage as Xe_n. This average Xe_n chemical shift is reproduced by the Monte Carlo simulations, for all the peaks for all the samples. In other words, the simulations find the correct fraction of cages that have an exact number of Xe atoms, and for those cavities having that number of Xe atoms, the simulations find the correct average number of Ar or CH_4 in the same cavity. In the special case of Xe-Kr mixtures, the mixed Xe_nKr occupancy is directly observed since individual peaks can be observed with either zero or one Kr atom with each Xe_n..

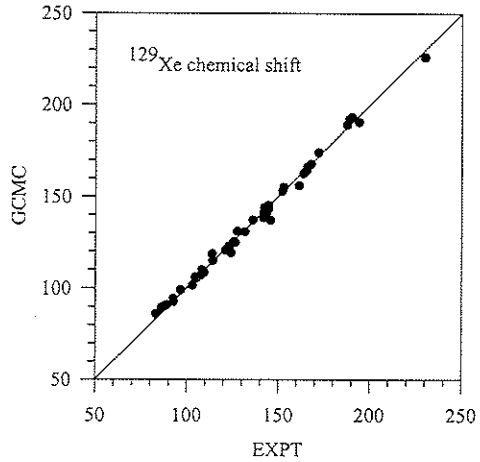

Figure 1. ^{129}Xe chemical shifts of Xe_n with CH_4 under fast exchange in zeolite Na*A*, obtained from GCMC simulations, compared with experimental values. The shifts are in ppm relative to the isolated Xe atom.

This is possible because both Xe and Kr have long residence times in a specific cavity. The Ar or CH_4 molecule is freely exchanging between cavities but the Xe_n chemical shift reports the average number of Ar or CH_4 with Xe_n, thus providing a more complete picture of distribution of mixed adsorbed species within a zeolite than has ever been obtained before.

We have investigated the effect of the cation on the chemical shifts and on the adsorption by observing Xe adsorbed in Na*A* in which all of the Na ions have been exchanged with K (zeolite K*A*) (*26*), and in Na*A* in which only some of the Na ions have been exchanged with Ca^{2+} ions (*28*). In the latter, we have been able to obtain the chemical shifts of Xe_n in cages containing no Ca (i.e., pure zeolite Na*A*), in cages containing one Ca and in cages containing two and three Ca ions. Each of these types of cages provides its own signature in the form of a progression of peaks giving the intensity distribution according to the Xe_n occupancies of cages of that particular type, and the Xe_n chemical shifts that are unique to that type of cage. The GCMC simulations support the assignments and provide a measure of the role of polarization of Xe by di and monvalent cations. We have also interpreted the ^{129}Xe NMR observations of Xe in Ag*A* by Moudrakovski, Ratcliffe and Ripmeester. (*27*) using the same GCMC simulations (*49*). The behavior of Xe_n in Ag*A* is very similar to that of Xe_n in Na*A*, and the interpretation is similarly successful. The observation of Xe_n chemical shifts in the same zeolite framework with differing cations Na^+, K^+, Ag^+, and Ca^{2+}, permit the interpretation of the physisorption of Xe in the A type zeolite in a quantitative way. Since the occupancy of each cage is directly observable, the chemical shifts are therefore clearly associated with a fixed number of Xe atoms in a cage which has the same framework atoms in the same arrangement, while at the same time permitting a variation in the type of cations present. In this way, detailed comparisons of simulation predictions of distributions and chemical shifts against experiments are possible. We have been able to understand how the type, size, and locations of cations affect the distribution of molecules within a cavity.

A more detailed picture of adsorption than ever before is made possible by the complete interpretation of the Xe_n chemical shifts, which, of course, is made possible by the use of ab initio intermolecular shielding functions. The excellent agreement of the simulation results with experiment in turn gives us confidence that the GCMC simulations are robust and the potential parameters being used are not too unreasonable. In this way, intermolecular shielding functions play a very important role in the fundamental understanding of adsorption. Without the chemical shifts, only an adsorption isotherm may be used for testing the simulations, and this quantity is a highly averaged physical quantity which only provides partitioning of the sorbate between inside and outside the zeolite. We on the other hand, have this inside-outside partitioning since we observe both the adsorbed and the bulk gas peaks, and we also have the detailed distributions of both types of sorbate molecules among the cavities of the zeolite. Temperature dependent studies have provided us with additional information about the one- and two-body distributions of the *n* Xe atoms within a cavity (*50*). The Xe-zeolite part of the average Xe_n chemical shift is a function of the one body distribution of the Xe in the cavity and the Xe-Xe part of the average Xe_n chemical shift is a function of the two-body Xe-Xe distribution function.

Our group and the Pines group have measured for Xe in zeolite Na*A*, via magnetization transfer and 2D-EXSY, the individual rate constants for a Xe atom

leaving a cage containing *n* Xe atoms, going into an adjacent cage containing (m-1) Xe atoms, for all *n* and *m* ranging from 1 to 8 (*51, 52*). A similar measurement has been made by Ripmeester's group for Xe in zeolite Ag*A* (*27*). The set of microscopic rate constants provide a very detailed picture of the diffusion of Xe atoms within the zeolite, that is, from the rate constants, the difussion coefficient for a sample at any average loading can be obtained. It is the large chemical shifts separating the Xe_n clusters that make such direct NMR measurements of microscopic rates possible.

Conclusions

We have investigated various mixtures in zeolite Na*A* as model systems for competitive adsorption in microporous solids. This work provides a more detailed comparison of experiment with GCMC simulations than has ever been possible. When we observed experimentally the clusters of *n* Xe atoms and *m* Kr atoms in the same cage, it was the first instance where the number of molecules of the second sorbate occupying the same cage as *n* atoms of the first sorbate have actually been determined. The Xe_n and the mixed Xe_nKr_m clusters are trapped in the alpha cages of this zeolite for times sufficiently long that it is possible to observe individual peaks in the NMR spectrum for each cluster. The ^{129}Xe chemical shift of the Xe_nKr_m peak is a measure of the distribution of the *n* Xe and *m* Kr atoms within the alpha cage. The absolute chemical shifts for the Xe_n and Xe_nKr peaks observed at 300 K, spanning a 200 ppm range, are in excellent agreement with the average chemical shifts for these mixed clusters in the GCMC simulations. ^{129}Xe chemical shift increments upon addition of one Kr atom to the Xe_n cluster are increasing monotonically with cluster size. A significant conclusion, which may be very helpful in competitive adsorption cases where such detailed comparisons with experiment are not feasible, is that the magnitude of the increments can be estimated semi-quantitatively from the known gas phase shifts in mixtures of Xe and Kr and from the Xe_n cluster shift increments. Similar observations, have been possible for other mixtures such as Xe-Ar and Xe-CH_4, except that in these cases, the Ar or CH_4 are in fast echange among the cages, so that only an average number of molecules occupying the same cage as an Xe_n is observed, and the Xe_n chemical shift is a direct measure of this average number. In these cases, the chemical shift of the Xe_n for every n, in all samples containing various mole fractions of Xe and other sorbate are reproduced very well by the GCMC simulations, thus permitting the complete interpretation of distributions and chemical shifts. Similarly, the Xe-CO, Xe-N_2, Xe-CO_2 shielding functions recently calculated by us (*36*) will provide a similar opportunity for interpretation of the competitive adsorption of these mixtures in zeolite Na*A*, using the NMR measurements that we have already carried out in these systems. Furthermore, the Xe chemical shifts in any open network zeolites, where only a single adsorbed peak signal can be obtained under fast Xe exchange can also be interpreted using the same simulations (*53*).

Acknowledgments

The research described here has been supported by the National Science Foundation (Grants No. CHE-9210790 and CHE-9528066) and the University Scholar program of the University of Illinois Foundation.

Literature Cited

1. *Zeolites and Related Microporous Materials: State of the Art 1994;* Weitkamp, J.; Kärge, H. G.; Pfeifer, H.; Hölderich, W., Eds.; Studies in Surface Science and Catalysis; Elsevier: Amsterdam, 1994; Vol.84.
2. Fraissard, J.; Ito, T. *J. Chem. Phys.* **1982,** *76,* 5225.
3. Fraissard, J.; Ito, T. *Zeolites* **1988,** *8,* 350.
4. Dybowski, C.; Bansal, N.; Duncan, T. M. *Ann. Rev. Phys. Chem.* **1991,** *42,* 433.
5. Barrie, P. J.; Klinowski, J. *Prog. NMR Spectrosc.* **1992,** *24,* 91.
6. Stengle, T. R.; Williamson, K. L. *Macromolecules* **1987,** *20,* 1428.
7. Miller, J. B.; Walton, J. H.; Roland, C. M. *Macromolecules* **1993,** *26,* 5602.
8. Kentgens, A. P. M.; van Boxtel, H. A.; Verweel, R. J.; Veeman, W. S. *Macromolecules* **1991,** *24,* 3712.
9. Suh, D. J.; Park, T. J.; Ihm, S. K.; Ryoo, R. *J. Phys. Chem.* **1991,** *95,* 3767.
10. Barrie, P. J.; McCann, G. F.; Gameson, I.; Rayment, T.; Klinowski, J. *J. Phys. Chem.* **1991,** *95,* 9416.
11. Cheung, T. T. P. *J. Phys. Chem.* **1989,** *93,* 7549.
12. Derouane, E. G.; Nagy, J. B. *Chem. Phys. Lett.* **1987,** *137,* 341.
13. Demarquay, J.; Fraissard, J. *Chem. Phys. Lett.* **1987,** *136,* 314.
14. Johnson, D. W.; Griffiths, L. *Zeolites* **1987,** *7,* 484.
15. Ripmeester, J. A.; Ratcliffe, C. I.; Tse, J. S. *J. Chem. Soc., Faraday Trans. 1* **1988,** *84,* 3731.
16. Kim, J.-G.; Kompany, T.; Ryoo, R.; Ito, T.; Fraissard, J. *Zeolites* **1994,** *14,* 427.
17. Wu, J. F.; Chen, T. L.; Ma, L. J.; Lin, M. W.; Liu, S. B. *Zeolites* **1992,** *12,* 86.
18. Chmelka, B. F.; Pearson, J. G.; Liu, S. B.; Ryoo, R.; de Menorval, L. C.; Pines, A. *J. Phys. Chem.* **1991,** *95,* 303.
19. Liu, S. B.; Fung, B. M.; Yang, T. C.; Hong, E. C.; Chang, C. T.; Shih, P. C.; Tong, F. H.; Chen, T. L. *J. Phys. Chem.* **1994,** *98,* 4393.
20. Boddenberg, B.; Hartmann, M. *Chem. Phys. Lett.* **1993,** *203,* 243.
21. Fraissard, J.; Kärger, J. *Zeolites* **1989,** *9,* 351.
22. Barrage, M. C.; Bonardet, J. L.; Fraissard, J. *Catal. Lett.* **1990,** *5,* 43.
23. Maistriau, L.; Derouane, E. G.; Ito, T. *Zeolites* **1990,** *10,* 311.
24. Jameson, C. J.; Jameson, A. K.; Gerald II, R. E.; de Dios, A. C. *J. Chem. Phys.* **1992,** *96,* 1676.
25. Chmelka, B. F.; Raftery, D.; McCormick, A. V.; de Menorval, L. C.; Levine, R. D.; Pines, A. *Phys. Rev. Lett.* **1991,** *66,* 580.
26. Jameson, C. J.; Jameson, A. K.; Gerald II, R. E.; Lim, H.-M. *J. Chem. Phys.* **1995,** *103,* 8811
27. Moudrakovski, I; Ratcliffe, C. I.; Ripmeester, J. A. *J. Am. Chem. Soc.* **1998,** *120,* 3123.
28. Jameson, A. K.; Jameson, C. J.; de Dios, A. C.; Oldfield, E.; Gerald II, R. E.; Turner, G. L. *Solid State Nucl. Magn. Reson.* **1995,** *4,* 1.
29. Jameson, C. J.; Jameson, A. K.; Lim, H.-M. *J. Chem. Phys.* **1997,** 107, 4364.
30. Jameson, C. J.; Jameson, A. K.; Lim, H.-M. *J. Chem. Phys.* **1996,** *104,* 1709.
31. Jameson, C. J.; de Dios, A. C. *J. Chem. Phys.* **1992,** *97,* 417
32. Jameson, C. J.; de Dios, A. C. *J. Chem. Phys.* **1993,** *98,* 2208.

33. Malkin, V. G.; Malkina, O. L.; Steinebrunner, G.; Huber, H. *Chemistry Eur. J.*, **1996**, *2*, 452.
34. Chesnut, D. B.; Rusiloski, B. E. *J. Mol. Struct. (THEOCHEM)* **1994**, *314*, 19.
35. *Nuclear Magnetic Shieldings and Molecular Structure*; Tossel, J. A., Ed.; NATO ASI Series C; Kluwer: Dordrecht, 1993, Vol. 386.
36. de Dios, A. C.; Jameson, C. J. *J. Chem. Phys.* **1997**, *107*, 4253.
37. Jameson, C. J.; Lim, H.-M. *J. Chem. Phys.* **1995**, *103*, 3885
38. Jameson, C. J.; Jameson, A. K.; Baello, B. I.; Lim, H.-M. *J. Chem. Phys.* **1994**, *100*, 5965.
39. Woods, G. B.; Rowlinson, J. S. *J. Chem. Soc., Faraday Trans. 2* **1989**, *85*, 765.
40. Aziz, R. A.; Slaman, M. J. *Mol. Phys.* **1986**, *57*, 825.
41. Aziz, R. A.; van Dalen, A. *J. Chem. Phys.* **1983**, *78*, 2402.
42. Aziz, R. A.; Slaman, M. J. *Mol. Phys.* **1986**, *58*, 679.
43. Liuti, G.; Pirani, F.; Buck, U.; Schmidt, B. *Chem. Phys.* **1988**, *126*, 1.
44. Righini, R.; Maki, K.; Klein, M. L. *Chem. Phys. Lett.* **1981**, *80*, 301.
45. Pluth, J. J.; Smith, J. V. *J. Am. Chem. Soc.* **1980**, *102*, 4704.
46. Allen, M. P.; Tildesley, D. J. *Computer Simulation of Liquids;* Clarendon: Oxford, 1987.
47. Jameson, C. J.; Jameson, A. K.; Kostikin, P.; Baello, B. I., to be published
48. Jameson, C. J.; Lim, H.-M.; Jameson, A. K. *Solid State Nucl. Magn. Reson.* **1997**, *9*, 277.
49. Jameson, C. J.; Lim, H. M. *J. Chem. Phys.* **1997**, *107*, 4373.
50. Jameson, C. J.; Jameson, A. K.; Lim, H.-M.; Baello, B. I. *J. Chem. Phys.* **1994**, *100*, 5977.
51. Jameson, A. K.; Jameson, C. J.; Gerald II, R. E. *J. Chem. Phys.*, **1994**, *101*, 1775.
52. Larsen, R. G.; Shore, J.; Schmidt-Rohr, K.; Emsley, L.; Long, H.; Pines, A.; Janicke, M.; Chmelka, B. F., *Chem Phys. Lett.*, **1993**, *214*, 220.
53. Jameson, C. J.; Jameson, A. K.; Gerald II, R. E.; Lim, H.-M. *J. Phys. Chem.* **1997**, *101*, 8418.